

Reaction mechanisms for $0.5\text{Li}_2\text{MnO}_3 \cdot 0.5\text{LiMn}_{0.5}\text{Ni}_{0.5}\text{O}_2$ precursor prepared by low-heating solid state reaction

Dong Li¹⁾, Fang Lian¹⁾, Xin-mei Hou²⁾, and Kuo-chih Chou^{1,2)}

1) School of Materials Science and Engineering, University of Science and Technology Beijing, Beijing 100083, China

2) Department of Physical Chemistry, University of Science and Technology Beijing, Beijing 100083, China

(Received: 18 January 2012; revised: 6 March 2012; accepted: 26 March 2012)

Abstract: Lithium-excess manganese layered oxides, which are commonly described in chemical formula $0.5\text{Li}_2\text{MnO}_3 \cdot 0.5\text{LiMn}_{0.5}\text{Ni}_{0.5}\text{O}_2$, were prepared by low-heating solid state reaction. The reaction mechanisms of synthesizing precursors, the decomposition mechanism, and intermediate materials in calcination were investigated by means of Fourier transform infrared spectroscopy (FT-IR), X-ray diffraction (XRD), field emission scanning electron microscopy (FESEM), thermogravimetric analysis (TGA), and differential scanning calorimetry (DSC). The major diffraction patterns of $0.5\text{Li}_2\text{MnO}_3 \cdot 0.5\text{LiMn}_{0.5}\text{Ni}_{0.5}\text{O}_2$ powder calcinated at 720°C for 15 h are indexed to the hexagonal structure with a space group of $R\bar{3}m$, and the clear splits of doublets at (006)/(102) and (108)/(110) indicate that the sample adopts a well-layered structure. FESEM images show that the size of the agglomerated particles of the sample ranges from 100 to 300 nm.

Keywords: lithium batteries; electrode; manganese oxide; solid state reactions; calcination

[This work was financially supported by the National High-Tech Research and Development Program of China (No.2009AA03Z226), the National Natural Science Foundation of China (No.50702007), the Fundamental Research Funds for the Central Universities (No.FRF-MP-12-005B), and the Special Funds for Excellent Doctoral Dissertation of Beijing (No.YB20081000801).]

1. Introduction

Over the last few years, much work has been devoted to the structures and properties of LiMnO_2 [1-4], $\text{LiMn}_{0.5}\text{Ni}_{0.5}\text{O}_2$ [5] and $\text{LiMn}_{0.333}\text{Ni}_{0.333}\text{Co}_{0.333}\text{O}_2$ [6] compounds because layered lithium manganese oxides are promising cathode materials for lithium secondary batteries in terms of abundance, cost, and nontoxicity. Among all these systems, Mn-based lithium-excess layered oxides with a formula of $x\text{Li}_2\text{MnO}_3 \cdot (1-x)\text{LiMn}_y\text{M}_{1-y}\text{O}_2$ ($0 < x < 1$, $0 < y < 1$, and M represents one or more transitional metal elements) are more attractive. Due to the high theoretical specific capacity and a discharge capacity above 200 mAh/g, the successful application of $x\text{Li}_2\text{MnO}_3 \cdot (1-x)\text{LiMn}_y\text{M}_{1-y}\text{O}_2$ can potentially increase the energy density of Li-ion batteries.

Presently, Li-excess cathode materials have been synthesized *via* various routes, such as the ion exchange method

[7], coprecipitation method [8-9], sol-gel method [10], hydrothermal method [11], solid state method [12], rheological similarity method [13], and combustion method [14]. Nevertheless, low-heating solid state synthesis has been assumed as one of the most innovative methods for simplicity and low-energy consumption (materials synthesized by only one step sintering) [15-16]. Besides, some problems in the process of other preparations can be avoided. For example, OH^- and CO_3^{2-} are frequently chosen as precipitants to precipitate transition metal ions in the process of coprecipitation. When OH^- or CO_3^{2-} was added into the solution of transition metal ions (Mn^{2+} , Ni^{2+} , and Co^{2+}), transition metal ions were not completely precipitated, but a part of metal ions and precipitates will lose during the process of washing precipitates. By comparison, composite stoichiometry is exactly controlled though low-heating solid state synthesis because of the simple preparation process.

Corresponding author: Fang Lian E-mail: lianfang@mater.ustb.edu.cn

© University of Science and Technology Beijing and Springer-Verlag Berlin Heidelberg 2012

From the structural point of view, in the low-heating solid state reaction, the crystal water is released during the mixing process of raw materials, which causes the raw materials to be in a 'melted' state. Therefore, as compared to the conventional solid state preparation, the diffusion of molecules in the state becomes easier, and the reaction can be carried out at low temperature.

In order to improve the electrochemical performance of Li-excess manganese layered oxides, the structures have to be investigated. Among the factors that control the structures, reaction mechanisms of preparation are essential. Although some reports about the cathode materials synthesized by the low-heat solid state reaction were given [17], reaction mechanisms of the synthesis precursor during the preparation process of Li-excess manganese layered oxides by the low-heating solid state reaction are still obscure. In this paper, the reaction mechanisms of synthesizing $0.5\text{Li}_2\text{MnO}_3 \cdot 0.5\text{LiMn}_{0.5}\text{Ni}_{0.5}\text{O}_2$ precursor through the low-heating solid-state reaction were investigated. In addition, the decomposition mechanism of $0.5\text{Li}_2\text{MnO}_3 \cdot 0.5\text{LiMn}_{0.5}\text{Ni}_{0.5}\text{O}_2$ precursor and intercalation materials in the process of being heated from room temperature to 1000°C were discussed.

2. Experimental

2.1. Synthesis

The mixture of stoichiometric $\text{C}_2\text{H}_2\text{O}_4 \cdot 2\text{H}_2\text{O}$ ($\geq 99.5\text{wt}\%$), $\text{LiOH} \cdot \text{H}_2\text{O}$ ($\geq 95\text{wt}\%$), $\text{C}_4\text{H}_6\text{NiO}_4 \cdot 4\text{H}_2\text{O}$ ($\geq 98\text{wt}\%$), and $\text{C}_4\text{H}_6\text{MnO}_4 \cdot 4\text{H}_2\text{O}$ ($\geq 99\text{wt}\%$) was milled for 2 h to obtain paste precursors. The $0.5\text{Li}_2\text{MnO}_3 \cdot 0.5\text{LiMn}_{0.5}\text{Ni}_{0.5}\text{O}_2$ precursor after spray drying was calcinated at different temperatures (250 , 319 , 346 , 500 , and 720°C) for 2 h in air followed by furnace cooling to room temperature. The $0.5\text{Li}_2\text{MnO}_3 \cdot 0.5\text{LiMn}_{0.5}\text{Ni}_{0.5}\text{O}_2$ cathode materials were prepared at 720°C for 15 h.

In order to analyze whether the composition of precursors contains LiHC_2O_4 , LiHC_2O_4 was synthesized by dissolving $\text{H}_2\text{C}_2\text{O}_4 \cdot 2\text{H}_2\text{O}$ in hot water and adding an equivalent mole amount of $\text{Li}_2\text{C}_2\text{O}_4$ and was dried at 100°C for 2 h.

2.2. Measurements of thermal properties

The thermal decomposition processes of the precursors were investigated in air by means of a thermal analysis instrument (SDT Q600, V20.9 Build 20).

2.3. Structure and morphology characterization

Powder X-ray diffraction (XRD, Japan, Rigaku, D/max-RB, 12 kW) using $\text{Cu K}\alpha$ radiation was employed to identify the

crystalline phase of the synthesized materials. Infrared spectra were recorded by Fourier transform infrared spectroscopy (FT-IR, Nicolet Nexus 670). Field emission scanning electron microscopy (FESEM, Germany, ZEISS, SUPRA, 55) was performed to study the morphology and particle size of $0.5\text{Li}_2\text{MnO}_3 \cdot 0.5\text{LiMn}_{0.5}\text{Ni}_{0.5}\text{O}_2$ obtained.

3. Results and discussion

3.1. XRD analysis of precursor

To investigate the reaction mechanism of composites in the process of milling, the precursor dried was analyzed by XRD. Fig. 1 also shows that the precursor includes a lot of amorphous materials. XRD characteristic peaks of the raw materials (manganese acetate and nickel acetate) disappear, while the strong diffraction peaks of LiHC_2O_4 appear with some weak diffraction peaks of $\text{LiHC}_2\text{O}_4 \cdot \text{H}_2\text{O}$. X-ray diffraction patterns of the precursor indicate that paste precursor dried consists of amorphous chelate, LiHC_2O_4 , and $\text{LiHC}_2\text{O}_4 \cdot \text{H}_2\text{O}$.

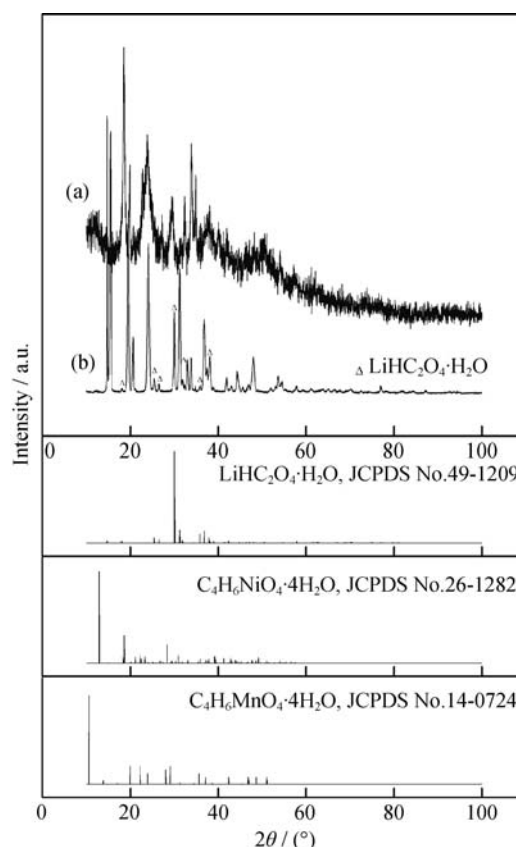


Fig. 1. XRD patterns of the precursor (a) and LiHC_2O_4 samples (b).

As shown in Fig.1, there are some weak peaks in the diffraction patterns of LiHC_2O_4 prepared in the experiment,

which is indexed to $\text{LiHC}_2\text{O}_4 \cdot \text{H}_2\text{O}$ of JCPDS No.49-1209. The work of Villepin and Novak [18] shows that LiHC_2O_4 do not absorb water at room temperature, it can be inferred that the drying time of crystals is not long enough to prepare pure anhydrous LiHC_2O_4 , which makes the low-heating solid state reaction and the thermal decomposition of precursors become more complex. However, compared with the precursor including LiHC_2O_4 , the investigation of the precursor including $\text{LiHC}_2\text{O}_4 \cdot \text{H}_2\text{O}$ is practical because it is difficult to remove all the crystal water in experiments and in industrial production.

3.2. FT-IR analysis of precursor

In order to further analyze the structure of amorphous chelates, FT-IR was employed. The Fourier transform infrared spectra of the $0.5\text{Li}_2\text{MnO}_3 \cdot 0.5\text{LiMn}_{0.5}\text{Ni}_{0.5}\text{O}_2$ precursor

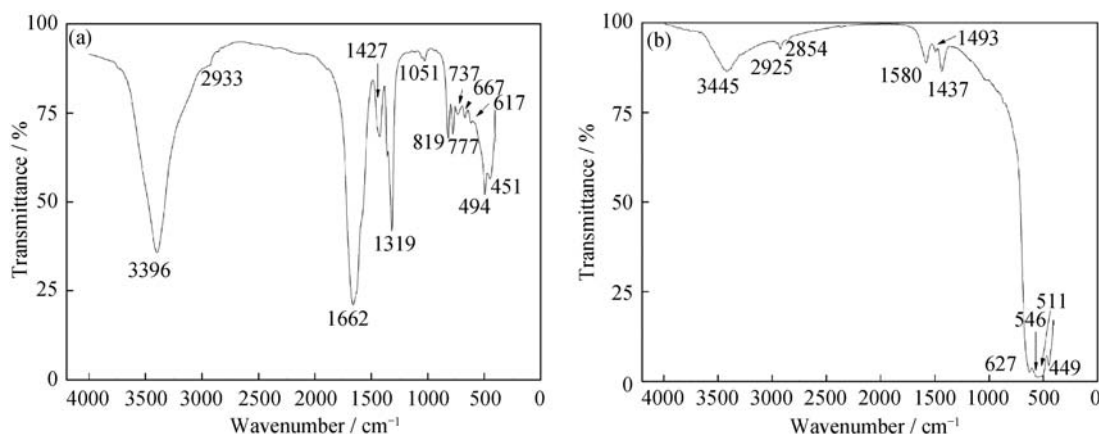


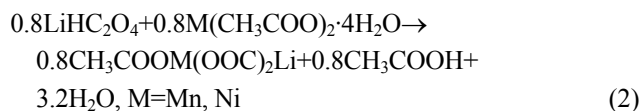
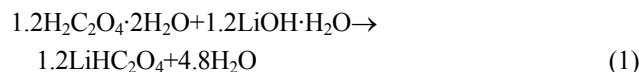
Fig. 2. FT-IR absorption spectra of $0.5\text{Li}_2\text{MnO}_3 \cdot 0.5\text{LiMn}_{0.5}\text{Ni}_{0.5}\text{O}_2$ cathode materials: (a) precursor; (b) calcinated powder.

Table 1. FT-IR spectra of the precursor and cathode materials

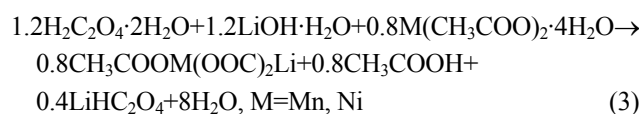
Wavenumber / cm^{-1}	Assignments	Precursor	Cathode materials
3396 [19-20]	O-H	×	—
3445/1580	H_2O (adsorbed)	—	×
2933	C-H	×	—
1622/1427	C=O, COO^-	×	—
1493/1437/546	Ni-O	—	×
1317/1051/819 [21]	C-COO	×	—
777/737/667/617/494 [21]	M-O (M=Ni, Mn)	×	—
627/511 [20, 22-23]	M-O	—	×
451 [23-25]	Li-O	×	—
449	Li-O	—	×

Note: × means containing the corresponding wavenumber.

and the sintered powder are shown in Figs. 2(a) and 2(b), respectively. Wavenumbers and assignments of the peaks are listed in Table 1. Based on the analysis of the Infrared spectra and XRD patterns, the reaction process of synthesizing the $0.5\text{Li}_2\text{MnO}_3 \cdot 0.5\text{LiMn}_{0.5}\text{Ni}_{0.5}\text{O}_2$ ($\text{Li}_{1.2}\text{Mn}_{0.6}\text{Ni}_{0.2}\text{O}_2$) precursor could be expressed as follows:



Combining Eqs. (1) and (2), one obtains



There are no COO and C=O groups in the infrared spectra of $0.5\text{Li}_2\text{MnO}_3 \cdot 0.5\text{LiMn}_{0.5}\text{Ni}_{0.5}\text{O}_2$ powder (Table 1), which indicates no residual oxalates, acetates, and carbonates in the cathode powder. The supposition can be also confirmed from the XRD patterns of the cathode powder.

3.3. Structural analysis of decomposition products and thermal analysis of precursor

According to thermogravimetric analysis (TGA) and differential scanning calorimetry (DSC) curves in Fig. 3, it can be seen that the prepared precursor decomposes in four stages as a result of dehydration, dehydroxylation, and decarburization, with the rearrangement of material structure. The process is accompanied by two endothermic peaks and a sharp exothermic peak. To confirm the decomposition products at different temperatures, the precursor is calcinated at the corresponding temperature, and decomposition products are characterized by XRD.

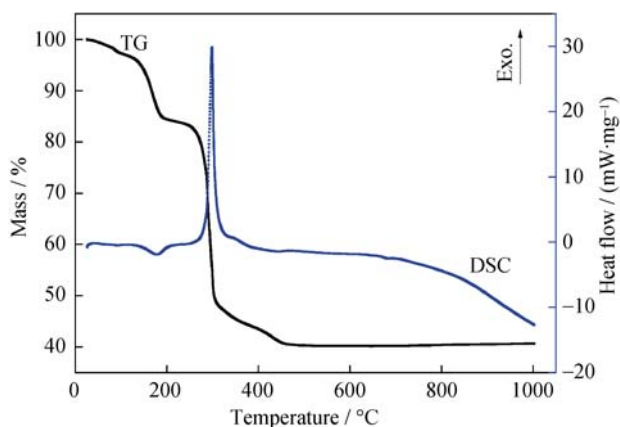


Fig. 3. TGA-DSC curves of the precursor at a heating rate of $10 \text{ K} \cdot \text{min}^{-1}$.

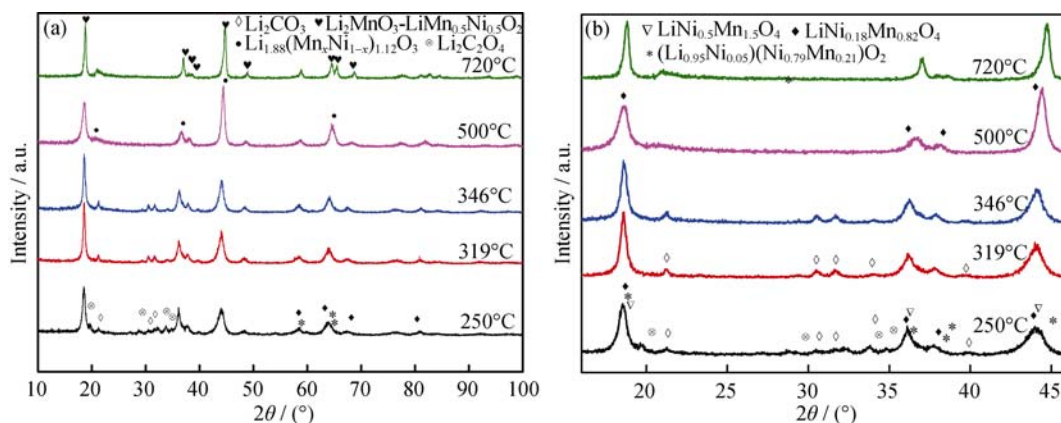


Fig. 4. XRD patterns of $0.5\text{Li}_2\text{MnO}_3 \cdot 0.5\text{LiMn}_{0.5}\text{Ni}_{0.5}\text{O}_2$ precursor calcinated at different temperatures (a) and the magnified patterns with the 2θ ranging from 16 to 46° .

As shown in Fig. 4, compared with the sample at 250°C , there are no obvious changes in the XRD patterns of the samples calcinated at 319 and 346°C except that the diffraction peaks of $\text{Li}_2\text{C}_2\text{O}_4$ disappear. It can be deduced that residual $\text{Li}_2\text{C}_2\text{O}_4$ decomposes completely. Due to this reaction, Fig. 3 shows that there is a sharp exothermic peak in the range.

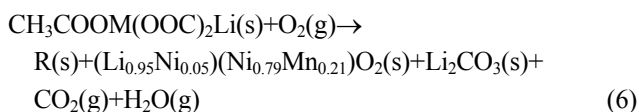
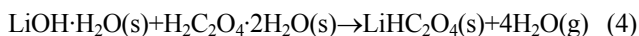
The XRD pattern of the sample calcinated at 500°C in Fig. 4(b) shows that decomposition products do not consist of Li_2CO_3 . It can be illustrated in the TG-DSC curves (Fig. 3). There is little weight loss accompanying a small endothermic peak in Fig. 3, which results from Li_2CO_3 being decomposed into Li_2O and CO_2 [27]. However, there are no characteristic peaks of Li_2O in the patterns of the sample. It can be inferred that Li_2O reacts with other decomposition products to form solid solution. Fig. 4(b) shows that compared with the sample calcinated at 250°C , the intensity of diffraction peaks of the samples appearing at $2\theta=18.5^\circ$ calcinated at 319 and 346°C are higher. With increasing the

The first stage is observed in the temperature range from 45 to 135°C . Mass loss is most probably corresponding to the release of adsorbed water, a little of acetic acid, and crystal water from $\text{LiHC}_2\text{O}_4 \cdot \text{H}_2\text{O}$ [25].

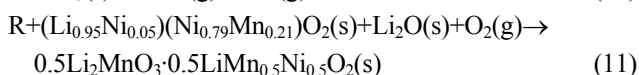
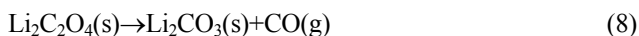
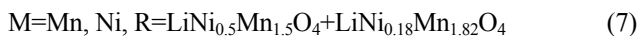
The second stage of decomposition is observed in the temperature range from 135 to 250°C , and Fig. 4 shows that the corresponding products at 250°C consists of $\text{Li}_2\text{C}_2\text{O}_4$, Li_2CO_3 , $(\text{Li}_{0.95}\text{Ni}_{0.05})(\text{Ni}_{0.79}\text{Mn}_{0.21})\text{O}_2$, and R ($\text{R}=\text{LiNi}_{0.5}\text{Mn}_{1.5}\text{O}_4 + \text{LiNi}_{0.18}\text{Mn}_{0.82}\text{O}_4$). It is deduced that LiHC_2O_4 [26] and amorphous chelate in Eq. 3 decompose completely in the process. Fig. 4(a) also shows that $\text{Li}_2\text{C}_2\text{O}_4$ begins to decompose at 250°C . In addition, all the peaks can be indexed based on a spinel structure except some weak diffraction peaks of $\text{Li}_2\text{C}_2\text{O}_4$, Li_2CO_3 , and $(\text{Li}_{0.95}\text{Ni}_{0.05})(\text{Ni}_{0.79}\text{Mn}_{0.21})\text{O}_2$.

temperature continuously, the intensity of diffraction peaks of the sample at 500°C becomes weaker, and the position of diffraction peaks appearing at $2\theta=44^\circ$ has a small deviation, which is attributed to the formation of new phase $\text{Li}_{1.88}(\text{Mn}_x\text{Ni}_{1-x})_{1.112}\text{O}_3$. In Fig. 3, it is clear that no further mass loss and thermal effect are observed, even though the temperature is heated to 1000°C . The XRD pattern of the sample calcinated at 720°C for 2 h in Fig. 4(a) shows that all the peaks can be indexed on the basis of layered $\alpha\text{-NaFeO}_2$ structure. The weak reflection peak appearing between 20 and 25° shows the characteristic of complex $\text{Li}_2\text{MnO}_3\text{-LiMO}_2$ phase resulting from the order of metal ions (Li^+ , Mn^{4+} , and Ni^{2+} ions in the transition metal layers) and the existence of Li_2MnO_3 [28]. It is deduced that when the sample was heated from 500 to 720°C , solid solution was obtained by the diffusion of transition metal and lithium ions in oxides.

The associated reactions for these processes can be expressed as follows:



where



3.4. Structure and morphology analysis of cathode powder

The XRD pattern of $0.5\text{LiMn}_2\text{O}_3\cdot 0.5\text{LiMn}_{0.5}\text{Ni}_{0.5}\text{O}_2$ calcinated at 720°C for 15 h in Fig. 5 shows that all the peaks can be indexed based on a hexagonal $\alpha\text{-NaFeO}_2$ structure with a space group of $R\bar{3}m$ [28-31]. The clear splitting of (006, 102) and (108, 110) [32-33] indicates that the sample with a well-development layered structure was prepared by low-heating solid state reaction.

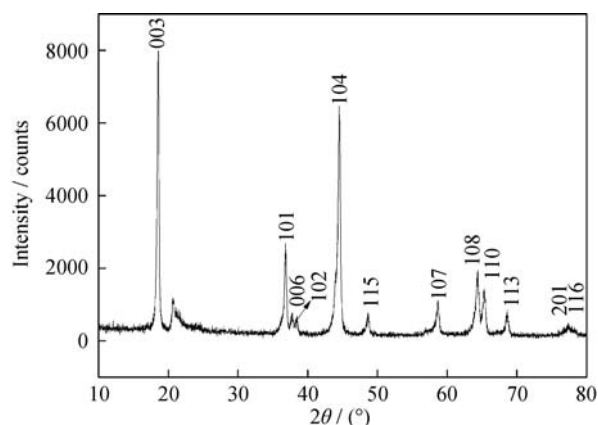


Fig. 5. XRD pattern of $0.5\text{Li}_2\text{MnO}_3\cdot 0.5\text{LiMn}_{0.5}\text{Ni}_{0.5}\text{O}_2$ precursor calcinated at 720°C for 15 h.

FESEM was performed to investigate the morphology and particle size of $0.5\text{Li}_2\text{MnO}_3\cdot 0.5\text{LiMn}_{0.5}\text{Ni}_{0.5}\text{O}_2$ power calcinated at 720°C for 15 h. Figs. 6(a) and 6(b) show that the size of the agglomerated particles of the sample ranges from 100 to 300 nm. Fig. 6 shows that the sample consists of agglomerated particles with the submicrometer diameter, which is attributed to the large specific surface area and high specific surface energy.

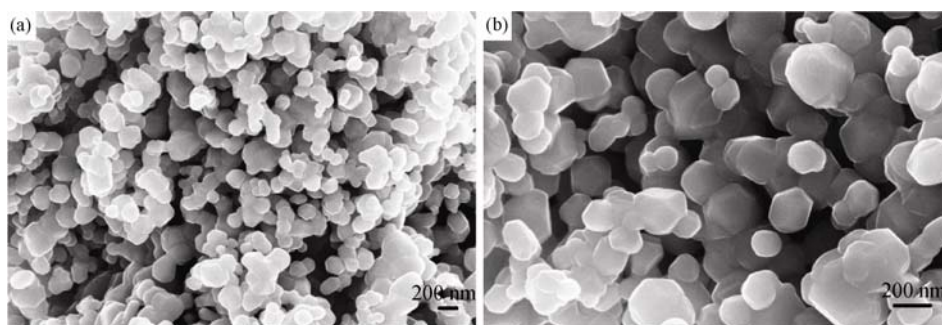


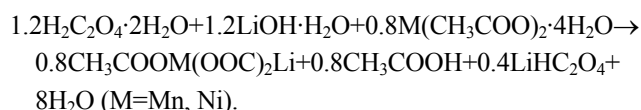
Fig. 6. FESEM images of $0.5\text{Li}_2\text{MnO}_3\cdot 0.5\text{LiMn}_{0.5}\text{Ni}_{0.5}\text{O}_2$ precursor calcinated at 720°C for 15 h.

According to Refs. [34-36], Li-excess manganese layered oxides $x\text{Li}_2\text{MnO}_3\cdot (1-x)\text{LiMn}_y\text{M}_{1-y}\text{O}_2$ ($\text{M}=\text{Ni}, \text{Co}$) were usually prepared at $800\text{-}1000^\circ\text{C}$. Compared with the literatures, the low-heating solid state method with the characterization of simple process, precise stoichiometry, and low sintering temperature is a promising route to industrial production of Li-excess manganese layered oxides.

4. Conclusions

(1) The $0.5\text{Li}_2\text{MnO}_3\cdot 0.5\text{LiMn}_{0.5}\text{Ni}_{0.5}\text{O}_2$ precursor was prepared by the low-heating solid state reaction, and the reaction processes of synthesizing the precursor were investi-

gated by XRD and FT-IR. The associated reaction could be expressed as



(2) The decomposition process and intermediate materials in the calcination were investigated and confirmed.

(3) After the precursor was calcinated at 720°C for 15 h, $0.5\text{Li}_2\text{MnO}_3\cdot 0.5\text{LiMn}_{0.5}\text{Ni}_{0.5}\text{O}_2$ cathode materials with a well-development layered structure were obtained. FESEM images show that the agglomerated particle sizes of the powder distribute between 100-300 nm.

References

- [1] I.J. Davidson, R.S. McMillan, J.J. Murray, and J.E. Greedan, Lithium-ion cell based on orthorhombic LiMnO₂, *J. Power Sources*, 54(1995), No.2, p.232.
- [2] G. Fan, Y. Zeng, R. Chen, and G. Lü, Microstructure and electrochemical characterization of spherical-like orthorhombic LiMnO₂ via co-precipitation, *J. Alloys Compd.*, 461(2008), No.1-2, p.267.
- [3] Z.P. Guo, G.X. Wang, K. Konstantinov, H.K. Liu, and S.X. Dou, Electrochemical properties of orthorhombic LiMnO₂ prepared by one-step middle-temperature solid-state reaction, *J. Alloys Compd.*, 346(2002), No.1-2, p.255.
- [4] S.J. Hwang, H.S. Park, J.H. Choy, and G. Campet, Evolution of local structure around manganese in layered LiMnO₂ upon chemical and electrochemical delithiation/re lithiation, *Chem. Mater.*, 12(2000), p.1818.
- [5] N.K. Karan, J.J. Saavedra-Arias, D.K. Pradhan, R. Melgarejo, A. Kumar, R. Thomas, and R.S. Katiyar, Structural and electrochemical characterizations of solution derived LiMn_{0.5}Ni_{0.5}O₂ as positive electrode for li-ion rechargeable batteries, *Electrochem. Solid State Lett.*, 11(2008), No.8, p.A135.
- [6] T.H. Cho, Y. Shiosaki, and H. Noguchi, Preparation and characterization of layered LiMn_{1/3}Ni_{1/3}Co_{1/3}O₂ as a cathode material by an oxalate co-precipitation method, *J. Power Sources*, 159(2006), No.2, p.1322.
- [7] N. Yabuuchi, K. Yoshii, S.T. Myung, I. Nakai, and S. Komaba, Detailed studies of a high-capacity electrode material for rechargeable batteries, Li₂MnO₃-LiMn_{1/3}Ni_{1/3}-Co_{1/3}O₂, *J. Am. Chem. Soc.*, 133(2011), No.12, p.4404.
- [8] F. Lian, P. Axmann, C. Stinner, Q.G. Liu, and M. Wohlfahrt-Mehrens, Comparative study of the preparation and electrochemical performance of LiNi_{1/2}Mn_{1/2}O₂ electrode material for rechargeable lithium batteries, *J. Appl. Electrochem.*, 38(2008), p.613.
- [9] T. Wang, Z.H. Liu, L.H. Fan, Y.F. Han, and X.H. Tang, Synthesis optimization of Li_{1+x}[Mn_{0.45}Co_{0.40}Ni_{0.15}]O₂ with different spherical sizes via co-precipitation, *Powder Technol.*, 187(2008), No.2, p.124.
- [10] J.H. Kim and Y.K. Sun, Electrochemical performance of Li[Li_xNi_{(1-3x)/2}Mn_{(1+x)/2}]O₂ cathode materials synthesized by a sol-gel method, *J. Power Sources*, 119-121(2003), p.166.
- [11] X.K. Huang, Q.S. Zhang, H.T. Chang, J.L. Gan, H.J. Yue, and Y. Yang, Hydrothermal synthesis of nanosized LiMnO₂-Li₂MnO₃ compounds and their electrochemical performances, *J. Electrochem. Soc.*, 156(2009), No.3, p.A162.
- [12] K. Numata, C. Sakaki, and S. Yamanaka, Synthesis and characterization of layer structured solid solutions in the system of LiCoO₂-Li₂MnO₃, *Solid State Ionics*, 117(1999), No.3-4, p.257.
- [13] G.Z. Wei, X. Lu, F.S. Ke, L. Huang, J.T. Li, Z.X. Wang, Z.Y. Zhou, and S.G. Sun, Crystal habit-tuned nanoplate material of Li[Li_{1/3-2x/3}Ni_xMn_{2/3-x/3}]O₂ for high-rate performance Lithium-Ion batteries, *Adv. Mater.*, 22(2010), No.39, p.4364.
- [14] Y.J. Park, Y.S. Hong, X.L. Wu, K.S. Ryu, and S.H. Chang, Structural investigation and electrochemical behaviour of Li[Li_{1/3-2x/3}Ni_xMn_{2/3-x/3}]O₂ compounds by a simple combustion method, *J. Power Sources*, 129(2004), No.2, p.288.
- [15] L.Y. Yu, W.H. Qiu, F. Lian, J.Y. Huang, and X.L. Kang, Understanding the phenomenon of increasing capacity of layered 0.65Li[Li_{1/3}Mn_{2/3}]O₂·0.35LiMn_{1/3}Ni_{1/3}Co_{1/3}O₂, *J. Alloys Compd.*, 471(2009), No.1-2, p.317.
- [16] L.Y. Yu, W.H. Qiu, F. Lian, W. Liu, X.L. Kang, and J.Y. Huang, Comparative study of layered 0.65 Li[Li_{1/3}Mn_{2/3}]O₂·0.35LiMO₂(M=Co, Ni_{1/2}Mn_{1/2} and Mn_{1/3}Ni_{1/3}Co_{1/3}) cathode materials, *Mater. Lett.*, 62(2008), No.17-18, p.3010.
- [17] J. Liu, W. Qiu, L. Yu, H. Zhao, and T. Li, Synthesis and electrochemical characterization of layered LiMn_{1/3}Ni_{1/3}Co_{1/3}O₂ cathode materials by low-temperature solid-state reaction, *J. Alloys Compd.*, 449(2008), No.1-2, p.326.
- [18] J. de Villepin and A. Novak, Liaison hydrogène O-H-O symétrique: II. Spectres de vibration des oxalates acides de lithium hydratés et anhydres, *J. Mol. Struct.*, 30(1976), p.255.
- [19] J. Hu, N. Jia, J.X. Jiang, M.G. Ma, J.F. Zhu, R.C. Sun, and J.Z. Li, Hydrothermal preparation of boehmite-doped AgCl nanocubes and their characterization, *Mater. Lett.*, 65(2011), No.11, p.1531.
- [20] S.Y. Yang, X.Y. Wang, J.L. Wei, X.Q. Li, and A.P. Tang, Synthesis and electrochemical performance of Na-Mn-O cathode materials, *Acta Phys. Chim. Sin.*, 24(2008), No.9, p.1669.
- [21] K. Nakamoto, Y. Morimoto, and A.E. Martell, Infrared spectra of metalchelate compounds V effect of substituents on the infrared spectra of metal acetylacetonates, *J. Chem. Phys.*, 66(1962), p.346.
- [22] P. Suresh, A.K. Shukla, and N. Munichandraiah, Characterization of Zn- and Fe-substituted LiMnO₂ as cathode materials in Li-ion cells, *J. Power Sources*, 161(2006), No.2, p.1307.
- [23] C.M. Julien and M. Massot, Lattice vibrations of materials for lithium rechargeable batteries: I. Lithium manganese oxide spinel, *Mater. Sci. Eng. B*, 97(2003), No.3, p.217.
- [24] P. Tarte and J. Preudhomme, ⁶Li-⁷Li isotopic shifts in the infrared spectrum of inorganic lithium compounds: II. Rhombohedral LiXO₂ compounds, *Spectrochim. Acta*, 26(1970), p.747.
- [25] P. Tarte, Identification of Li-O bands in the infra-red spectra of simple lithium compounds containing LiO₄ tetrahedra, *Spectrochim. Acta*, 20(1964), No.2, p.238.
- [26] T.F. Du and S.J. Zhang, Studies on the thermal decomposition of potassium hydrogen oxalate monohydrate by combined thermal analysis and gas chromatography, *Chin. J. Inorg. Chem.*, 15(1999), p.531.
- [27] X.H. Hu, X.P. Ai, H.X. Yang, and S.X. Li, A study of LiMn₂O₄ synthesized from Li₂CO₃ and MnCO₃, *J. Power Sources*, 74(1998), No.2, p.240.
- [28] A.R. Armstrong, M. Holzapfel, P. Novak, C.S. Johnson, S.H. Kang, M.M. Thackeray, and P.G. Bruce, Demonstrating oxygen loss and associated structural reorganization in the

- Lithium battery cathode $\text{Li}[\text{Ni}_{0.2}\text{Li}_{0.2}\text{Mn}_{0.6}]\text{O}_2$, *J. Am. Chem. Soc.*, 128(2006), p.8694.
- [29] J. Ryu, B. Park, S. Kim, and Y. Park, Effects of surface area on electrochemical performance of $\text{Li}[\text{Ni}_{0.2}\text{Li}_{0.2}\text{Mn}_{0.6}]\text{O}_2$ cathode material, *J. Appl. Electrochem.*, 39(2009), No.7, p.1059.
- [30] B.J. Hwang, C.J. Wang, C.H. Chen, Y.W. Tsai, and M. Venkateswarlu, Electrochemical properties of $\text{Li}[\text{Ni}_x\text{Li}_{(1-2x)/3}\text{Mn}_{(2-x)/3}]\text{O}_2$ ($0 \leq x \leq 0.5$) cathode materials prepared by a sol-gel process, *J. Power Sources*, 146(2005), No.1-2, p.658.
- [31] M.M. Thackeray, S.H. Kang, C.S. Johnson, J.T. Vaughey, R. Benedek, and S.A. Hackney, Li_2MnO_3 -stabilized LiMO_2 (M=Mn, Ni, Co) electrodes for lithium-ion batteries, *J. Mater. Chem.*, 17(2007), p.3112.
- [32] C. Julien, G.A. Nazri, and A. Rougier, Electrochemical performances of layered $\text{LiM}_{1-y}\text{M}'_y\text{O}_2$ (M=Ni, Co; M'=Mg, Al, B) oxides in lithium batteries, *Solid State Ionics*, 135(2000), No.1-4, p.121.
- [33] K.M. Shaju, G.V. Subba Rao, and B.V.R. Chowdari, Performance of layered $\text{LiMn}_{1/3}\text{Ni}_{1/3}\text{Co}_{1/3}\text{O}_2$ as cathode for Li-ion batteries, *Electrochim. Acta*, 48(2002), No.2, p.145.
- [34] J.H. Lim, H. Bang, K.S. Lee, K. Amine, and Y.K. Sun, Electrochemical characterization of Li_2MnO_3 - $\text{LiMn}_{1/3}\text{Ni}_{1/3}\text{Co}_{1/3}\text{O}_2$ - LiNiO_2 cathode synthesized via co-precipitation for lithium secondary batteries, *J. Power Sources*, 189(2009), No.1, p.571.
- [35] F. Weill, N. Tran, L. Croguennec, and C. Delmas, Cation ordering in the layered $\text{Li}_{1+x}(\text{Ni}_{0.425}\text{Mn}_{0.425}\text{Co}_{0.15})_{1-x}\text{O}_2$ materials ($x=0$ and 0.12), *J. Power Sources*, 172(2007), No.2, p.893.
- [36] M.M. Thackeray, S.H. Kang, C.S. Johnson, J.T. Vaughey, and S.A. Hackney, Comments on the structural complexity of lithium-rich $\text{Li}_{1+x}\text{M}_{1-x}\text{O}_2$ electrodes (M=Mn, Ni, Co) for lithium batteries, *Electrochem. Commun.*, 8(2006), p.1531.